

A nuclear configuration interaction approach to study nuclear spin effects: an application to *ortho*- and *para*- $^3\text{He}_2@\text{C}_{60}$

Félix Moncada,^[a, d] William Quintero,^[b, d] Edwin Posada,^[c, d] Lars G. M. Pettersson,^[a] and Andrés Reyes^{*[d]}

We introduce a non-orthogonal configuration interaction approach to investigate nuclear quantum effects on energies and densities of confined fermionic nuclei. The Hamiltonian employed draws parallels between confined systems and many-electron atoms, where effective non-Coulombic potentials represent the interactions of the trapped particles. One advantage of this method is its generality, as it offers the potential to study the nuclear quantum effects of various confined species affected by effective isotropic or anisotropic potentials.

As a first application, we analyze the quantum states of two ^3He atoms encapsulated in C_{60} . At the Hartree–Fock level, we observe the breaking of spin and spatial symmetries. To ensure

wavefunctions with the correct symmetries, we mix the broken-symmetry Hartree–Fock states within the non-orthogonal configuration interaction expansion.

Our proposed approach predicts singly and triply degenerate ground states for the singlet (*para*- $^3\text{He}_2@\text{C}_{60}$) and triplet (*ortho*- $^3\text{He}_2@\text{C}_{60}$) nuclear spin configurations, respectively. The *ortho*- $^3\text{He}_2@\text{C}_{60}$ ground state is 5.69 cm^{-1} higher in energy than the *para*- $^3\text{He}_2@\text{C}_{60}$ ground state. The nuclear densities obtained for these states exhibit the icosahedral symmetry of the C_{60} embedding potential. Importantly, our calculated energies for the lowest 85 states are in close agreement with perturbation theory results based on a harmonic oscillator plus rigid rotor model of $^3\text{He}_2@\text{C}_{60}$.

Introduction

Nuclear quantum effects span a variety of phenomena, including zero-point energy, molecular vibrations, tunneling, and isotope effects.^[1–3] These effects play a fundamental role in diverse disciplines, such as chemistry, biology, physics, and materials science. The study of nuclear quantum effects is crucial as it permits attaining a more accurate description and prediction of atomic, molecular, and condensed matter behavior.^[4–10]

In contrast, certain nuclear quantum effects, specifically nuclear spin effects (NSEs), have a more subtle influence on the

physical properties of matter.^[11,12] Still, these NSEs play a crucial role in techniques such as nuclear magnetic resonance^[13] and electron paramagnetic resonance,^[14] which are widely employed for exploring molecular structure and properties. Similarly, accurately assigning rovibrational spectroscopic measurements depends on the proper understanding of NSEs.^[15] Nuclear spin multiplicity influences the energy separation of quantum states. For instance, the rovibrational spectra of molecular hydrogen display an energy splitting of 118.9 cm^{-1} between the ground states of *ortho*-H₂ (*o*-H₂, with triplet H spin configuration) and *para*-H₂ (*p*-H₂, with singlet H spin configuration).^[16] Similar energy splittings have been observed for the two nuclear spin isomers of water in the gas phase. Here, the ground state of *ortho*-water exhibits an energy 23.8 cm^{-1} higher than that of *para*-water.^[17]

NSEs extend beyond hydrogen-containing systems and can impact the properties of systems comprising multiple identical nuclei.^[18] For instance, numerous investigations on pure and doped nanoclusters comprising ^3He and ^4He , have analyzed how different helium nuclear spin configurations affect their spectroscopic properties and superfluidity.^[19–22] Furthermore, experimental reports on doped clusters reveal NSEs on He atoms are brought closer together by condensation on molecules such as OCS,^[23] SF₆^[24] or aromatic hydrocarbons.^[25]

Alternatively, the proximity of He atoms can be enforced by confining them within a molecular cage, such as a fullerene. Experimental results have demonstrated the presence of one and two helium atoms trapped inside fullerenes using spectroscopic techniques.^[26–29] Numerous theoretical investigations employing molecular mechanics and electronic structure ap-

[a] F. Moncada, L. G. M. Pettersson
Department of Physics, AlbaNova University Center,
Stockholm University,
106 91, Stockholm (Sweden)

[b] W. Quintero
Doctorado en Fisicoquímica Molecular,
Universidad Andres Bello,
Santiago de Chile (Chile)

[c] E. Posada
Institute for Computational Molecular Science,
Temple University
Philadelphia, PA (USA)

[d] F. Moncada, W. Quintero, E. Posada, A. Reyes
Department of Chemistry, Universidad Nacional de Colombia,
Av. Cra 30 45-03, Bogotá (Colombia)
E-mail: areyesv@unal.edu.co

 Supporting information for this article is available on the WWW under
<https://doi.org/10.1002/cphc.202300498>

Pablo Villarreal Herrán Festschrift

proaches have analyzed various phenomena exhibited in systems with one and two He atoms trapped within C_{60} .^[30–35] In particular, it has been shown that helium atoms within C_{60} exhibit a lower rotational barrier compared to other noble gases, indicating their relatively unrestricted motion within the cage.^[36,37] Molecular dynamics simulations have also been utilized to incorporate the effects of temperature and analyze the classical distribution of nuclei.^[38] Nevertheless, these studies have overlooked the quantum nature of nuclei, resulting in the omission of analyses regarding the impact of NSEs on system properties.

Here, our primary objective is to develop a systematic Non-Coulombic (NC) Non-Orthogonal Configuration Interaction (NOCI) method to analyze NSEs in systems containing multiple identical nuclei. The NOCI approach has a lower formal scaling than full configuration interaction (FCI) and has been used in regular electronic structure^[39–41] and nuclear plus electronic structure calculations^[42] for systems where the Hartree–Fock (HF) method breaks the spin or spatial symmetry to lower the energy. It has been observed that by taking a linear combination of these broken-symmetry HF solutions, the NOCI can restore the static correlation and recover the correct symmetry of the wavefunction.^[41] The proposed NC-NOCI method allows us to study NSEs on the quantization of nuclear states without the need to consider translational, rotational, and vibrational separations of the nuclear degrees of freedom. Furthermore, the systematic nature of the NC-NOCI approach makes it applicable for analyzing the quantum states of particles or pseudo-particles trapped in cavities of diverse shapes.

As a first application of our NC-NOCI approach, we calculate the nuclear wavefunctions and energies of two ^3He atoms (referred to as He hereafter) confined in C_{60} ($\text{He}_2@C_{60}$). This system exhibits nuclear spin isomerism, forming either *para*- $\text{He}_2@C_{60}$ (*p*- $\text{He}_2@C_{60}$) or *ortho*- $\text{He}_2@C_{60}$ (*o*- $\text{He}_2@C_{60}$) with singlet or triplet spin configurations, respectively. Therefore, NSEs may impact the He_2 structure and dynamic behavior. When applied to $\text{He}_2@C_{60}$, our approach decouples the degrees of freedom of C_{60} from those of the encapsulated He atoms. Furthermore, the He atoms are treated as dressed nuclei. This approach draws inspiration from electronic structure methods. Under this setting, we construct an effective Hamiltonian that considers He dressed nuclei as interacting quantum waves embedded in an external field generated by the carbon atoms. Equivalent effective Hamiltonians have been employed to study He clusters formed around molecules,^[43–53] and inside carbon nanotubes.^[54]

To contrast the results obtained with the proposed NC-NOCI method, we adapt the perturbation theory (PT) approach from Ref. [55] to $\text{He}_2@C_{60}$. In that study, the PT approach was developed to analyze the translation-rotation structure of $\text{H}_2@C_{60}$, a system that is also composed of two fermionic nuclei with relatively unrestricted motion inside C_{60} . The PT results of Ref. [55] are in excellent agreement with extensive experimental and theoretical data regarding the splittings of the $\text{H}_2@C_{60}$ translation-rotation levels.^[56–67]

The structure of the paper is as follows: In the Theoretical and Computational Aspects section, we present the proposed

NC-NOCI approach and provide details of the numerical simulations. In the Results and Discussion section, we present the energies and densities obtained for two helium atoms trapped in C_{60} . Finally, in the Conclusions section, we provide final remarks summarizing the findings of this study.

Theoretical and Computational Aspects

From a quantum perspective, the calculation of the total wavefunction of two He atoms confined within C_{60} involves considering the degrees of freedom of 62 nuclei and 364 electrons.

Previous related studies have demonstrated that the dimensionality of the confined system can be significantly reduced by exploiting the minimal coupling between the motions of the confined species and those of C_{60} .^[68–71] Based on this approximation, the degrees of freedom of He_2 and C_{60} can be adiabatically separated. The dimensionality can be further reduced by recognizing that He_2 does not form chemical bonds with the walls of C_{60} or with each other. As a result, each confined ^3He atom can be treated as a dressed nucleus, possessing a formal charge of 0 and a nuclear spin $s=1/2$. The interactions between the He atoms and with the walls of C_{60} are accounted for through the utilization of effective potentials.

Due to the fermionic nature of He nuclei, approximate solutions of the time-independent Schrödinger equation, $\hat{H}\Psi = E\Psi$, can be obtained within a HF framework. This approach is analogous to the one utilized in studies of doped He clusters.^[43,45–49] In this context, the He wavefunction, Ψ^{He} , is represented by a Slater determinant composed of He spin-orbitals. It has been found that at the HF level, only high-spin configurations are properly described, whereas low-spin configurations must be described with a multiconfigurational approach.^[53] To overcome this limitation of the HF method and achieve an enhanced physical description, several dressed He nuclei studies have employed the FCI level and related multi-configurational schemes.^[48,50–54]

The confined $^3\text{He}_2$ system can exist in singlet ($S=0$, $p^3\text{He}_2$) or in triplet ($S=1$, $o^3\text{He}_2$) nuclear spin states. In the case of *p*- He_2 , the quantum statistics is properly accounted for by antisymmetrizing the spin component of the nuclear wavefunction. Consequently, the orbital part is symmetric, leading to doubly occupied orbitals when employing a single-determinant representation. It is important to note that any other choice of singly occupied orbitals would result in spin contamination. In contrast, for *o*- He_2 , antisymmetrization occurs in the orbital part, where two orbitals are singly occupied. Therefore, when employing a single-determinant representation, the spin component must be symmetric.

Non-Coulombic Non-Orthogonal Configuration Interaction (NC-NOCI)

To capture the quantum behavior of identical encapsulated nuclei, we develop a Hamiltonian analogous to the electronic

molecular Hamiltonian under the Born-Oppenheimer approximation. In this formulation, the nuclei of interest are treated as quantum particles, analogous to electrons, while the atoms comprising the encapsulating cage are considered fixed point-like particles. As a result, this Hamiltonian incorporates the nuclear kinetic energy, as well as the potential energy arising from the nucleus-nucleus and nucleus-cage interactions, expressed through effective pairwise potentials:

$$\hat{H} = -\sum_i^{N_q} \frac{\nabla_i^2}{2m_q} + \sum_i^{N_q} \sum_l^{N_p} \hat{V}_{qp}(\mathbf{r}_i - \mathbf{R}_l) + \sum_i^{N_q} \sum_{j>i}^{N_q} \hat{V}_{qq}(\mathbf{r}_i - \mathbf{r}_j) \quad (1)$$

Here, N_q is the number of quantum nuclei of mass m_q , N_p is the number of encapsulating point-like nuclei, \hat{V}_{qp} is a quantum point-like nuclei potential energy operator and \hat{V}_{qq} is a quantum-quantum nuclei potential energy operator. We use atomic units in this document and denote the energy and length units as E_h and a_0 respectively. In this section, we employ lowercase i, j as quantum nuclei indices and uppercase l as point-like nuclei index.

The wavefunction for identical fermionic nuclei in the HF representation is expressed as a single Slater determinant, which is an antisymmetrized product of spin-orbitals:^[72]

$$|\Psi_{HF}\rangle = \left| \prod_i^{N_q} \chi_i \right\rangle \quad (2)$$

Here, each spin-orbital χ_i is the product of an orbital ψ_i and a nuclear spin function. For a nuclear spin s , there are $2s+1$ orthonormal spin functions. Orbitals, ψ , are constructed as linear combinations of basis functions, and their combination coefficients are obtained by solving the one-particle Fock equations, $\hat{f}\psi_i = \varepsilon_i\psi_i$.

In the NC-NOCl approach, the wavefunction:

$$|\Psi_{NOCl}\rangle = \sum_A^{N_{conf}} C_A |\Psi_A\rangle, \quad (3)$$

is expressed as a linear combination of N_{conf} Hartree-Fock wavefunctions Ψ_A . Here, we use indices A and B as configuration iterators.

The energy diagonal matrix, \mathbf{E} , and combination coefficients matrix, \mathbf{C} , are determined by solving the NC-NOCl matrix equation:

$$\mathbf{H}^{NO} \mathbf{C} = \mathbf{S}^{NO} \mathbf{CE} \quad (4)$$

The elements of the NC-NOCl overlap, \mathbf{S}^{NO} , and Hamiltonian matrices, \mathbf{H}^{NO} , are evaluated following the method of Ref. [73]. An element S_{AB}^{NO} of \mathbf{S}^{NO} is computed as the determinant of the occupied orbitals overlap,

$$S_{AB}^{NO} = \langle \Psi_A | \Psi_B \rangle = |\mathbf{S}| \quad (5)$$

Here, \mathbf{S} is the overlap matrix between occupied orbitals that belong to configurations A and B . The elements, S_{ij} , of this matrix are of the form:

$$S_{ij} = \langle \psi_{i \in A} | \psi_{j \in B} \rangle \quad (6)$$

If $|\mathbf{S}| > 0$, the computed S_{AB}^{NO} terms are used to evaluate the elements, H_{AB}^{NO} , of \mathbf{H}^{NO} , as:

$$\begin{aligned} H_{AB}^{NO} &= \langle \Psi_A | \hat{H} | \Psi_B \rangle \\ &= S_{AB}^{NO} \left(\sum_{i \in A}^{N_q} \sum_{j \in B}^{N_q} \langle \psi_i | \hat{h}_q | \psi_j \rangle S_{ji}^{-1} \right. \\ &\quad \left. + \frac{1}{2} \sum_{i, i' \in A}^{N_q} \sum_{j, j' \in B}^{N_q} \langle \psi_i \psi_{i'} | \hat{V}_{qq} | \psi_j \psi_{j'} \rangle \left[S_{ji}^{-1} S_{j'i'}^{-1} - S_{ji'}^{-1} S_{j'i}^{-1} \right] \right) \end{aligned} \quad (7)$$

where S_{ji}^{-1} is an element of the occupied orbitals inverse matrix \mathbf{S}^{-1} . Here, the core operator, \hat{h}_q , is:

$$\hat{h}_q(\mathbf{r}) = -\frac{\nabla_r^2}{2m_q} + \sum_l^{N_p} \hat{V}_{ql}(\mathbf{r} - \mathbf{R}_l) \quad (8)$$

If $|\mathbf{S}| = 0$ extended Slater rules are applied.^[40]

Once the generalized eigenvalue problem is solved, the density matrices of the NC-NOCl states can be expressed in terms of the atomic orbital basis set employed in the NC-HF calculations. In this study, we propose employing the NC-NOCl approach to characterize the He₂@C₆₀ system.

He₂@C₆₀ effective potentials

We derive the nuclear Hamiltonian for the He₂@C₆₀ system from the general Hamiltonian in Eq. (1):

$$\hat{H}_{He_2@C_{60}} = -\sum_i^2 \frac{\nabla_i^2}{2m_{He}} + \sum_i^2 \hat{V}_{He_2@C_{60}}(\mathbf{r}_i) + \hat{V}_{He-He}(\mathbf{r}_{12}) \quad (9)$$

Here, $\hat{V}_{He_2@C_{60}}$ represents the effective interaction potential between each He and the C₆₀ walls, and \hat{V}_{He-He} denotes the He-He effective interaction potential.

To obtain the \hat{V}_{He-He} potential, calculations were performed at the CCSD(T)/aug-cc-pVnZ ($n=3-5$) level combined with the complete basis set (CBS) extrapolation technique.^[74] Various He-He internuclear distances \mathbf{r}_{12} were considered. The effective potential was determined by calculating the energy difference between the He dimer and two free He atoms, $V_{He-He}(\mathbf{r}_{12}) = E_{He-He}(\mathbf{r}_{12}) - 2E_{He}$. To simplify the calculation of matrix elements in the openLOWDIN code,^[75] the potential function was expanded using Gaussian type functions (GTFs):

$$\hat{V}_{He-He}(\mathbf{r}_{12}) = \sum_l^N c_l \exp(-\alpha_l \mathbf{r}_{12}^2) \quad (10)$$

The expansion coefficients, c_i , and exponents, α_i , of the GTFs are provided in Table S1 in the supporting information (SI). Figure S1 in the SI compares the fitted potentials and the CCSD(T) interaction energies.

Using the GTF expansion of $\hat{V}_{\text{He-He}}$, the elements of the NC-HF two-particle matrix are calculated from four-center integrals of the form:

$$\langle \mu\sigma | \hat{V}_{\text{He-He}} | \nu\lambda \rangle = \sum_i^N c_i \langle \mu\sigma | \exp(-\alpha_i r_{12}^2) | \nu\lambda \rangle \quad (11)$$

where μ , ν , σ , λ are GTF basis functions, and we employed the physicist's notation for the four-center integrals.^[72] These integrals are evaluated using the contracted Gaussian Geminal operator implemented in the latest version of the Libint library.^[76]

To construct the $\hat{V}_{\text{He@C}_60}$ potential, we followed several steps. First, the geometry of C_{60} was optimized at the B3LYPD3/def2-SVP level of theory, imposing the I_h point group. This optimized geometry was kept fixed in subsequent calculations. Next, MP2/cc-pVDZ level energy calculations were performed for a system comprising a He atom inserted into C_{60} . In these calculations, the He atom was gradually displaced along a line connecting the center-of-mass (CM) of C_{60} and the center of a hexagon face of the cage. At each displacement point, the interaction energy was computed as $\hat{V}_{\text{He@C}_60}(\mathbf{r}) = E_{\text{He@C}_60}(\mathbf{r}) - E_{\text{C}_60} - E_{\text{He}}$. These interaction energies were then fitted to a sum of Lennard-Jones (8–6) potential terms for each helium-carbon pair distance ($r = |\mathbf{r} - \mathbf{R}_i|$) in C_{60} , represented as $V_{\text{He-C}}(r) = A/r^8 - B/r^6$. The fitting procedure allowed us to determine the attractive ($A = 604.05 \text{ E}_h^{-8}$), and repulsive ($B = 17.17 \text{ E}_h^{-6}$) parameters.

To facilitate the evaluation of matrix elements in terms of a Gaussian basis set, the Lennard-Jones function was expressed as a linear combination of N Gaussian functions. The total $\hat{V}_{\text{He@C}_60}$ potential employed was of the form:

$$\hat{V}_{\text{He@C}_60}(\mathbf{r}) = \sum_i^{60} \sum_i^N c_i \exp(-\alpha_i (\mathbf{r} - \mathbf{R}_i)^2) \quad (12)$$

The expansion coefficients, c_i , and exponents, α_i , are provided in Table S2 along with the C_{60} coordinates (\mathbf{R}_i) in Table S3 in the SI. Figure S2 in the SI compares the fitted potentials and the MP2 interaction energies. By employing the GTF expansion of $\hat{V}_{\text{He@C}_60}$, the matrix elements of the NC-HF one-particle potential matrix are easily calculated from three-center overlap integrals,

$$\langle \mu | \hat{V}_{\text{He@C}_60} | \nu \rangle = \sum_i^{60} \sum_i^N c_i \langle \mu | \exp(-\alpha_i (\mathbf{r} - \mathbf{R}_i)^2) | \nu \rangle \quad (13)$$

Representation of the $\text{He}_2@\text{C}_{60}$ HF wavefunction

At the HF level, helium orbitals are constructed as linear combinations of a set of basis GTFs in two alternative ways. In the first, the basis set is centered at the CM of C_{60} , inspired by

the nearly spherical symmetry of C_{60} . Here, we employed 13 s-type and 13 p-type GTFs, with even-tempered exponents ranging from 10.0 to 0.10 a_0^{-2} .

In the second way, the basis set is centered on two centers (TC) symmetrically separated from the CM along a C_3 symmetry axis. This choice is inspired by electronic structure geometry optimization results reporting that the He-He separation inside C_{60} is around 3.7 a_0 and energy differences between orientations along any of the symmetry axis are negligible ($< 10^{-4} \text{ E}_h$).^[32]

To select the optimal TC basis parameters, we followed several steps. First, we placed two [1s] GTFs and minimized the energy with respect to their separation and exponent. Then, at this optimized position ($r = \pm 1.851 \text{ a}_0$), we performed calculations employing [1s1p], [1s1p1d] or basis sets. The exponents of these GTFs were also optimized and are presented in Table 1.

Procedure to generate the NC-NOCI configurations

To generate configurations, NC-HF calculations were performed using TC basis sets located at various positions. In view of the nearly spherical symmetry of C_{60} we selected the He basis set positions from Lebedev angular grids,^[77] with 110, 192, and 302 points, in a radius $r = 1.851 \text{ a}_0$, corresponding to the optimized HF center positions obtained from the previous step.

We propose a geometric criterion to reduce the number of configurations in the NC-NOCI expansion: a configuration is included only if the distance between its basis set centers d is $d_{\min} < d < 2r$, where d_{\min} is a cutoff and $2r$ is the maximum distance between points in the Lebedev grid. Figure 1 illustrates a schematic representation of the nearly spherical grid, showcasing the possible basis set combinations at a given d_{\min} value. The results of NC-NOCI calculations with different d_{\min} values were contrasted with NC-FCI outcomes obtained using the 110 grid of [1s] basis functions. In subsection we discuss the choice of an optimal d_{\min} value.

In NC-HF calculations, self-consistent field (SCF) convergence was achieved when the change in energy between two successive iterations reached a value lower than 10^{-10} E_h . In NC-NOCI calculations, Hamiltonian matrix elements are assigned a value of zero when the overlap of the corresponding configurations is lower than 10^{-8} .

The NC-HF and NC-NOCI methods were implemented in the openLOWDIN package,^[75] which is an open version branch of the LOWDIN software.^[78] The current implementation of the NC-HF and NC-NOCI supports multiple types of quantum particles

Table 1. Optimized He basis set exponents (a_0^{-2}) for NC-HF calculations in the two-center basis set approach ($r = \pm 1.851 \text{ a}_0$).

| <i>l</i> | [1s] | [1s1p] | [1s1p1d] | [1s1p1d1f] |
|----------|--------|--------|----------|------------|
| s | 3.8187 | 3.8373 | 4.8697 | 4.9789 |
| p | | 3.8185 | 2.6936 | 2.5311 |
| d | | | 3.4703 | 3.3983 |
| f | | | | 3.2064 |

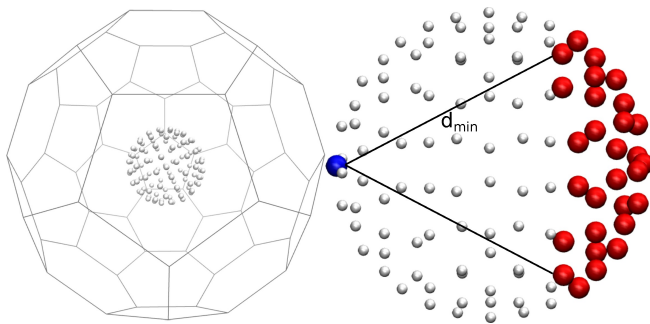


Figure 1. Schematic representation of the multicenter basis placement used in NC-NOCI calculations. From a Lebedev grid (in white) we select one point to position the first set of basis functions (shown in blue). Next, we select a second point at a minimum distance of d_{\min} to place the second basis set (indicated in red). NC-HF calculations are performed for every combination of these points.

following the Any Particle Molecular Orbital framework.^[79] All electronic structure calculations were carried out using the ORCA 5.0.3 package.^[80] Orbital and density plots were generated with the VMD software.^[81]

Perturbation theory reference model

To contrast the NC-HF and NC-NOCI results, we used a perturbation theory (PT) approach to compute the energy of $\text{He}_2@\text{C}_{60}$, considering only the six degrees of freedom of He_2 with the Hamiltonian of Eq. 9. This approach is closely related to the PT method described in Ref.^[55] to analyze the rotational and translational states of $\text{H}_2@\text{C}_{60}$.

We constructed a reference Hamiltonian, \hat{H}_0 , in CM ($\mathbf{R} = \mathbf{r}_1/2 + \mathbf{r}_2/2$, $R = |\mathbf{R}|$, $\Omega = \Theta, \Phi$), and internal ($\mathbf{s} = \mathbf{r}_2 - \mathbf{r}_1$, $s = |\mathbf{s}|$, $\omega = \theta, \phi$) spherical coordinates. \hat{H}_0 is composed by an isotropic 3D harmonic oscillator (HO) for the CM degrees of freedom, and a 1D HO for the internal distance coordinate,

$$\hat{H}_0 = -\frac{\nabla_{\mathbf{R}}^2}{4m_{\text{He}}} - \frac{\nabla_{\mathbf{s}}^2}{m_{\text{He}}} + k_{\text{r}} R^2 + k_s (s - s_{eq})^2 \quad (14)$$

From a potential scan setting $\mathbf{R}=0$ along a c_3 symmetry axis, shown in Figure S3. in the SI, we derive the values $k_s = 9.383 \times 10^{-3} \text{ E}_h/\text{a}_0^2$ and $s_{eq} = 3.658 \text{ a}_0$. Similarly, from a spherical average of the potential with $\mathbf{s} = \mathbf{s}_{eq}$, presented in Figure S4. in the SI, we computed $k_r = 6.034 \times 10^{-3} \text{ E}_h/\text{a}_0^2$.

To separate the internal distance and the angular equations, we assumed a rigid rotor (RR) approximation with a He_2 pseudo-molecule bond length equal to s_{eq} and a rotational constant of $B = m_{\text{He}}^{-1} s_{eq}^{-2} = 2.967 \text{ cm}^{-1}$. Under this RR framework, we separated our zeroth-order wavefunctions Ψ_0 as:

$$\Psi_0 = \psi_v(s)\psi_{nl}(R)A_{lj}^{\lambda\alpha}(\Omega, \omega) \quad (15)$$

Here, ψ_v is a 1D HO wavefunction, ψ_{nl} is the radial part of a 3D HO wavefunction, and $A_{lj}^{\lambda\alpha}$ is a linear combination of

products between CM and internal spherical harmonics, $Y_{mj}^l(\Omega)Y_{mj}^j(\omega)$. The angular wavefunctions resulting from this linear combination exhibit a well-defined total angular momentum, λ , obtained from the coupling of the CM \mathbf{l} and internal \mathbf{j} angular momentum vectors. The total angular momentum possible values are $\lambda = |l-j|, |l-j|+1, \dots, l+j$. In addition, the linear combination coefficients also anticipate the energy splitting of the spherical harmonics in an I_h potential. Additional details of the angular reference wavefunctions can be found in the SI.

With these definitions of \hat{H}_0 and Ψ_0 , we compute the first order PT corrected energy as the reference kinetic energy plus the expectation value of the potential operator:

$$\begin{aligned} E_1 &= \langle \Psi_0 | \hat{H}_{\text{He}_2@\text{C}_{60}} | \Psi_0 \rangle \\ &= \frac{\nu_R}{2} \left(n + \frac{3}{2} \right) + \frac{\nu_s}{2} \left(v + \frac{1}{2} \right) + Bj(j+1) \\ &\quad + \langle \Psi_0 | \hat{V}_{\text{He}_2@\text{C}_{60}} | \Psi_0 \rangle \end{aligned} \quad (16)$$

The frequencies of the HOs are $\nu_s = 573.6 \text{ cm}^{-1}$ and $\nu_R = 230.0 \text{ cm}^{-1}$. We computed the potential energy expectation value, by a 1D internal distance integral, $\langle \psi_v | \hat{V}_3 | \psi_v \rangle$ and a 5D translational and rotational integral, $\langle \psi_{nl} A_{lj}^{\lambda\alpha} | \hat{V}_{5D} | \psi_{nl} A_{lj}^{\lambda\alpha} \rangle$. As in Ref. [55], we have employed an expansion into bipolar spherical tensors of the potential to evaluate the 5D integrals. Details of the 5D expansion and 1D and 5D integral evaluation are presented in the SI.

Eq. (16) adds, via PT, anharmonicity and anisotropy effects to the HO plus RR reference. Energy predictions derived from Eq. (16) are denoted as PT-HORR energies. Specifically, we computed PT-HORR energies for the ground state ($v=0$) of the 1D HO, the first two radial functions ($nl=00, 11$) of the 3D HO, and the angular wavefunctions with $l=0, 1, j=0, 1, \dots, 9$ and $\lambda=0, 1, \dots, 9$.

Results and Discussion

NC-HF analysis

We conducted several NC-HF calculations for *o*- $\text{He}_2@\text{C}_{60}$ and *p*- $\text{He}_2@\text{C}_{60}$ configurations employing CM and TC basis set centers. The orbitals obtained employing the CM basis set are labeled according to the irreducible representations of the I_h group. On the other hand, the axis selection in the TC approach lowers the symmetry of the system from I_h to D_{2h} . Here, He_2 may be viewed as a linear molecule with an inversion center. Therefore, we use the $\sigma_{g/u}$ notation to refer to the TC orbitals.

Table 2 presents the NC-HF energies obtained for *o*- $\text{He}_2@\text{C}_{60}$ and *p*- $\text{He}_2@\text{C}_{60}$ configurations. For reference, it also includes the ground state energy computed with the PT-HORR model. For *p*- $\text{He}_2@\text{C}_{60}$ with the CM basis, we obtained a $|a_g^2\rangle$ ground state configuration with total energy 135 mE_h. With the TC basis, we

Table 2. He₂@C₆₀ NC-HF energy components (mE_h) for o-He₂@C₆₀ (³Ψ) and p-He₂@C₆₀ (¹Ψ) configurations. The potential energy minimum (*V*_{min}) and the energy obtained with the PT-HORR model are presented for reference.

| Configuration | Basis | Center ^[a] /a ₀ | E _{total} | $\langle \hat{K}_{\text{He}} \rangle$ | $\langle \hat{V}_{\text{He-He}} \rangle$ | $\langle \hat{V}_{\text{He@C}_60} \rangle$ |
|---|------------|---------------------------------------|--------------------|---------------------------------------|--|--|
| ¹ Ψ = a _g ² ⟩ | [13 s] | 0 | 134.729 | 0.843 | 94.122 | 39.764 |
| ¹ Ψ = σ _g ² ⟩ | [1s] | ± 1.851 | 1841.632 | 2.085 | 1836.274 | 3.273 |
| ³ Ψ = 1a _g 2a _g ⟩ | [13 s] | 0 | 48.426 | 1.990 | 29.003 | 17.433 |
| ³ Ψ = a _g t _{1u} ⟩ | [13 s13p] | 0 | 35.458 | 0.681 | 21.511 | 13.266 |
| ³ Ψ = σ _g σ _u ⟩ | [1s] | ± 1.851 | 8.213 | 2.085 | 2.855 | 3.273 |
| | [1s1p] | | 8.213 | 2.081 | 2.823 | 3.308 |
| | [1s1p1d] | | 7.667 | 1.792 | 2.619 | 3.256 |
| | [1s1p1d1f] | | 7.634 | 1.765 | 2.787 | 3.082 |
| <i>V</i> _{min} | – | ± 1.829 | 4.207 | – | 2.312 | 1.895 |
| PT-HORR | – | – | 7.151 | 1.466 | 2.843 | 2.842 |

[a] Two-center calculations were performed placing the basis sets along a C₃ axis. *V*_{min} was also located along a C₃ axis.

obtained a |σ_g²⟩ configuration with a total energy of 1842 mE_h.

Regardless of the choice of basis set centers, the calculated NC-HF energies for low-spin nuclear configurations are unphysically large compared to reference values from the PT-HORR model.

Unusual high energies have also been observed in HF calculations involving low-spin configurations of identical fermionic nuclei, such as of doped He₂ singlet systems,^[49] and the two ¹H nuclei in H₂.^[82] These high-energy outcomes are attributed to the limitations of single-configurational wavefunctions in describing singlet states. This is primarily due to the presence of large spurious self-repulsion integrals. In regular electronic calculations, these self-repulsion integrals also become problematic when describing the dissociation of a closed-shell molecule into open-shell fragments. For example, the dissociation of the H₂ molecule is not correctly described at the restricted HF level because the energy includes a one-center electron-electron repulsion integral unbalanced at larger distances.^[72]

On the other hand, self-repulsion integrals are absent from the HF energies of high-spin configurations.^[72,82] As a consequence, the ground state energies of o-He₂@C₆₀ presented in Table 2 are considerably lower than those of p-He₂@C₆₀,

irrespective of the basis set size and center. For the CM basis, the total energy of o-He₂@C₆₀ obtained with [13 s] GTFs 48.426 mE_h, is reduced to 35.458 mE_h, when the basis is expanded to [13 s13p] GTFs. These results are still considerably higher compared to the PT-HORR model one of 7.151 mE_h.

The TC basis set results for o-He₂@C₆₀ also show a gradual decrease in total energy as the number of basis functions with different angular momentum increases. Similar total energies are predicted with the [1s1p1d] and [1s1p1d1f] basis sets, 7.667 mE_h and 7.634 mE_h, respectively. These total energies are lower than those of the CM basis set and are comparable to that of the PT-HORR model. Further inspection of Table 2 reveals that the potential energy terms $\langle \hat{V}_{\text{He-He}} \rangle$ and $\langle \hat{V}_{\text{He@C}_60} \rangle$ are one order of magnitude larger for the CM basis results than for the TC basis results.

To gain insight on the potential energy difference between CM and TC results, Figure 2 depicts NC-HF orbitals for o-He₂@C₆₀. a_g and t_{1u} orbitals obtained with the CM basis set are more delocalized than σ_g and σ_u orbitals obtained with the TC basis set. The higher delocalization displayed by the CM orbitals indicates that the He atoms get closer to the walls of the C₆₀, thereby increasing their repulsion. Furthermore, the delocalized

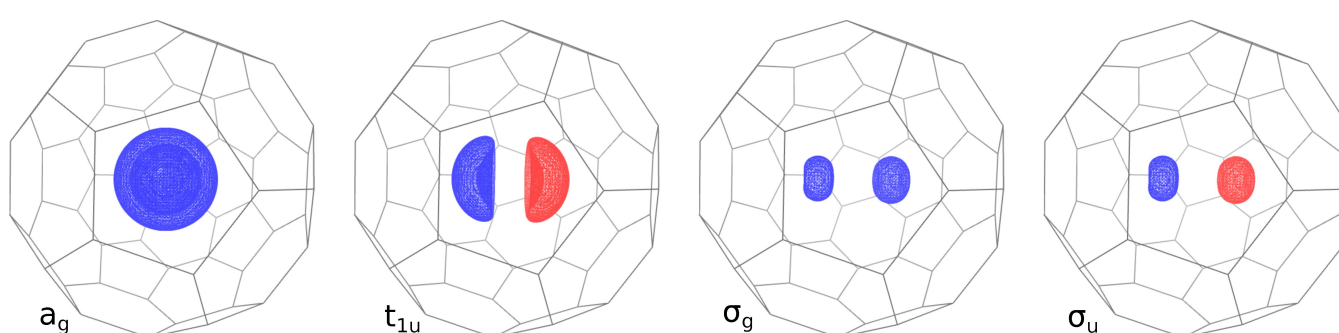


Figure 2. NC-HF orbitals for o-He₂@C₆₀ (triplet configurations). CM orbitals, a_g and t_{1u}, were obtained with a 13 s13p even-tempered basis set. TC orbitals, σ_g and σ_u, were obtained with optimized [1s1p1d] basis functions centered at ± 1.851 a₀. Contour values: ± 0.1 a₀^{-3/2}.

orbitals display a higher overlap, which in turn generates a higher He-He repulsion.

The NC-HF calculations are utilized as a reference for identifying the optimal size and centers of the basis set. The convergence of CM and TC calculations should yield equivalent energies upon reaching the complete basis set limit. Although we have not reached this limit, the NC-HF results obtained with a single-determinant wavefunction clearly predict a localized triplet ground state. The remaining calculations in this paper only consider the TC basis sets

When describing two helium atoms enclosed within C_{60} using TC orbitals, one approach to obtain physically meaningful energies for $p\text{-He}_2@C_{60}$ is to generate a spin-adapted configuration as a linear combination of two open-shell determinants.^[72] At the optimized distance of the TC basis sets, the overlap between these functions is negligible, resulting in minimal contribution from exchange integrals. Therefore, an open-shell wavefunction, $\Psi = |\sigma_g^a \sigma_u^\beta\rangle$, yields the same energy as the corresponding ${}^3\Psi$ state presented in Table 2. However, the reduced overlap also leads to the maximum possible spin contamination.^[72] This spin contamination is removed by employing a spin-adapted configuration, ${}^1\Psi = |\sigma_g^a \sigma_u^\beta\rangle - |\sigma_g^\beta \sigma_u^a\rangle$.

Spin-adapted configurations are explicitly considered within the NC-NOCI method by generating two open-shell singlet HF wavefunctions for each He-He TC orientation.

NC-NOCI energies

To initiate the NC-NOCI calculations, it is essential to determine the optimal value for the cutoff distance (d_{min}) between the TC basis functions. Figure 3 illustrates the variation in total NC-NOCI energies as a function of d_{min} , using [1s] basis sets distributed across a 110 point grid. Additionally, it includes NC-FCI results obtained using the same basis set. The figure reveals

that reducing d_{min} increases the number of NC-HF configurations included in the NC-NOCI expansion, resulting in the total energies converging towards the NC-FCI results. It also indicates that the singlet and triplet state energies converge at a similar rate as d_{min} decreases. Consequently, the NC-NOCI $o\text{-}p$ splitting achieves convergence with a smaller number of configurations compared to total energies.

Choosing the right value for d_{min} is crucial in NC-NOCI calculations. A smaller value brings the energy closer to the variational limit but significantly increases the computational cost, which scales quadratically with the number of configurations. The creation of the Hamiltonian matrix (H^{NO}) is a bottleneck for NC-NOCI calculations.

In our calculations, we chose $d_{min} = 3.6 a_0$, as shown in Figure 3. This selection ensures that the NC-NOCI energy is only $5 \times 10^{-6} E_h$ higher than the FCI energy. Importantly, with this d_{min} value, the NC-NOCI splitting closely approximates the FCI prediction, differing by only 0.002 cm^{-1} . This choice of d_{min} incorporates 758 configurations in the NC-NOCI expansion, accounting for only 6% of the total FCI configurations.

Table 3 presents the energies for $p\text{-He}_2@C_{60}$ and $o\text{-He}_2@C_{60}$ obtained with NC-NOCI and different combinations of grids and basis set sizes. As anticipated from the variational nature of the NC-NOCI method, the energies decrease as the number of basis set functions and grid points increase. Notably, increasing the number of basis functions yields a more significant reduction in energy compared to increasing the number of grid points. In contrast to NC-HF, the NC-NOCI method predicts that $o\text{-He}_2@C_{60}$ has higher energy than $p\text{-He}_2@C_{60}$. The NC-NOCI method predicts an $o\text{-}p$ energy splitting of 5.69 cm^{-1} with the basis and grid combination that leads to the lowest energies, [1s1p1d] GTFs in 194 points.

As reference values, Table 3 also displays the $p\text{-He}_2@C_{60}$ and $o\text{-He}_2@C_{60}$ energies and $o\text{-}p$ splitting predicted by the PT-HORR model. To compute these energies, we consider the symmetry of the spatial and spin wavefunctions. The ground state functions of the HO and RR ($j=0$) are symmetric, so the

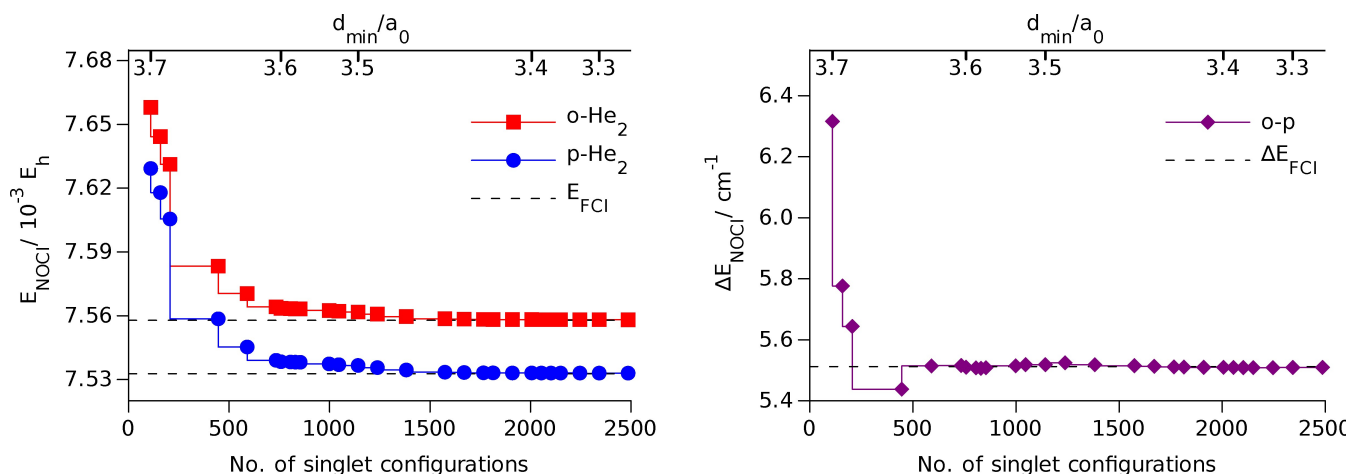


Figure 3. NC-NOCI ground state energies for $p\text{-He}_2@C_{60}$ and $o\text{-He}_2@C_{60}$ (left) and their difference (right) as a function of the number of HF configurations included in the CI expansion. The number of configurations is determined by the minimum separation between He basis functions, d_{min} . The number of triplet configurations mixed is half the number of singlet configurations. Calculations were performed with [1s] basis sets on the 110 point Lebedev grid with $r=1.851 a_0$. FCI results with the same basis set (12100 configurations) are presented for reference.

Table 3. Ground state energies (E) for $p\text{-He}_2@\text{C}_{60}$ and $o\text{-He}_2@\text{C}_{60}$ and their difference (ΔE) computed with NC-NOCl and NC-FCI employing different basis sets and Lebedev grids. All Lebedev grids use $r = 1.851 \text{ a}_0$, and all NC-NOCl calculations were performed with $d_{min} = 3.6 \text{ a}_0$. For reference, the PT-HORR model results are also presented.

| Method | Basis | No. centers | No. conf. ^[a] | $E(p\text{-He}_2)/\text{mE}_h$ | $E(o\text{-He}_2)/\text{mE}_h$ | $\Delta E/\text{cm}^{-1}$ |
|---------|----------|-------------|--------------------------|--------------------------------|--------------------------------|---------------------------|
| FCI | [1s] | 110 | 12100 | 7.533 | 7.558 | 5.51 |
| | [1s] | 194 | 37636 | 7.527 | 7.551 | 5.34 |
| NOCl | [1s] | 110 | 758 | 7.538 | 7.563 | 5.51 |
| | [1s] | 194 | 1850 | 7.528 | 7.552 | 5.34 |
| | [1s] | 302 | 5462 | 7.527 | 7.552 | 5.34 |
| | [1s1p] | 110 | 758 | 7.520 | 7.543 | 5.15 |
| | [1s1p] | 194 | 1850 | 7.502 | 7.525 | 5.05 |
| | [1s1p1d] | 110 | 758 | 7.261 | 7.288 | 5.79 |
| | [1s1p1d] | 194 | 1850 | 7.253 | 7.279 | 5.69 |
| PT-HORR | - | - | - | 7.151 | 7.178 | 5.93 |

[a] The number of triplet configurations mixed in the NC-NOCl expansion is half that of the singlet.

antisymmetry of the nuclear wavefunction is determined by the spin function of $p\text{-He}_2@\text{C}_{60}$ (nuclear spin $S = 0$). The first nuclear-excited state consists of the ground state HO functions combined with the $j=1$ state of the RR. Since the $j=1$ rotational wavefunction is antisymmetric, the antisymmetry of the nuclear wavefunction is preserved with a symmetric $o\text{-He}_2@\text{C}_{60}$ spin state ($S = 1$). Therefore, the energy of this first excited state differs from the ground state by the $j=1$ rotational energy ($2B$).

Consistent with the results of the PT-HORR model, our NC-NOCl analysis successfully predicts the correct spin symmetry of the ground nuclear state of $\text{He}_2@\text{C}_{60}$ and its $o\text{-}p$ splitting energy. The lowest NC-NOCl energies and the PT-HORR model results exhibit a difference of only 0.10 mE_h (1.4%) for both $p\text{-He}_2$ and $o\text{-He}_2$ states. Likewise, the $o\text{-}p$ splitting prediction differs by only 0.24 cm^{-1} between the two approaches.

The agreement between the predictions of both models strongly suggests that the NC-NOCl approach captures the correct physical description of the system. However, at this stage, we are unable to confirm which prediction is more accurate, as the PT theory is not variational. In the framework of the effective potentials we are utilizing, the accuracy in the calculation of total nuclear energy considering the PT-HORR model is impacted by the validity of the hamiltonian separation

used to decouple the translational, rotational, and vibrational degrees of freedom. In contrast, the accuracy of the NC-NOCl approach is impacted by the basis set incompleteness error. In addition, the NC-NOCl results converge to the NC-FCI only for [1s] basis sets. For larger basis sets, the NC-NOCl energies will converge to a higher value than the corresponding NC-FCI energy because the current NC-NOCl approach only mixes ground state NC-HF determinants.

NC-NOCl densities

Figure 4 displays the NC-NOCl ground state density of $p\text{-He}_2@\text{C}_{60}$. The panel with the highest contour value (0.088 a_0^{-3}) exhibits 20 density maxima. These maxima form an icosahedron, with their vertices pointing towards the hexagon faces of C_{60} . This is evidence of how the NC-NOCl wavefunction responds to the anisotropy of the $V^{\text{He-C}_{60}}$ potential, indicating the orientations with the highest likelihood of finding He atoms. However, as the contour values slightly decrease (below 0.06 a_0^{-3}), the other panels in Figure 4 demonstrate that the probability density becomes nearly spherical. Consequently, the probability of finding the He-He pseudo-molecule in any other direction within the system is significant. These results indicate

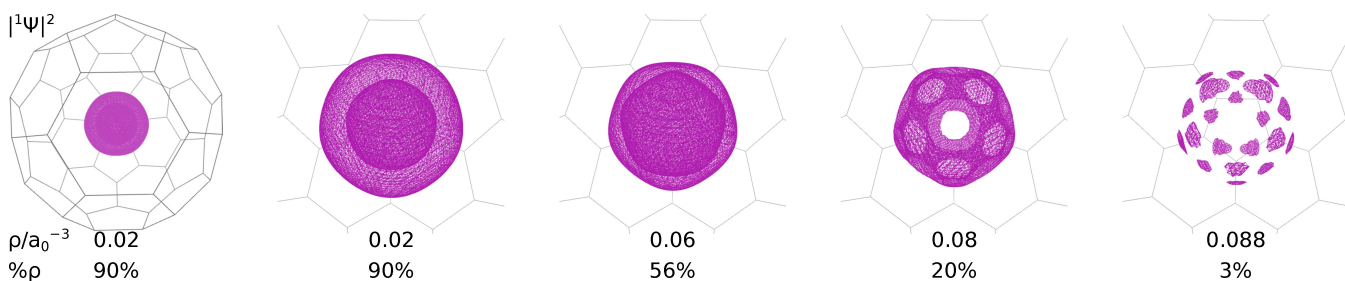


Figure 4. Density contours for the lowest energy NC-NOCl $p\text{-He}_2@\text{C}_{60}$ state. NC-NOCl calculations obtained from 194 possible He positions with the [1s1p1d] basis set.

that the He dimer has nearly free rotations inside the C_{60} even at 0 K.

Figure 5 presents the NC-NOCI density for the lowest-energy triply degenerate $o\text{-He}_2@C_{60}$ states. The displayed densities correspond to spatial wavefunctions of T_{1u} symmetry. The three $o\text{-He}_2$ states exhibit equivalent density distributions, each with two maxima along a preferred C_2 symmetry axis. These preferred axes pass through C=C (6-6) bonds of C_{60} and have 90° angles between them. Assuming a mixed state with equal probabilities for these three degenerate states, the resulting density becomes icosahedral, with 20 equivalent maxima symmetrically located along the 10 C_3 rotation axes of C_{60} , as shown in the bottom panel of Figure 5.

The nearly spherical densities shown in Figures 4 and 5 offer insights into the similarities between the NC-NOCI and the PT-HORR model results. In the quantum RR model, the solutions are represented using spherical harmonics. For $l=0, j=0$, the solution is a constant, indicating that every orientation has the same probability. Similarly, assuming that the three degenerate functions with $l=0, j=1$ are in a mixed state with equal probability, we obtain a radially symmetric density distribution.

The energies obtained from the PT-HORR and NC-NOCI approaches show remarkable agreement. This is also consistent with the similarity between the spherical densities predicted

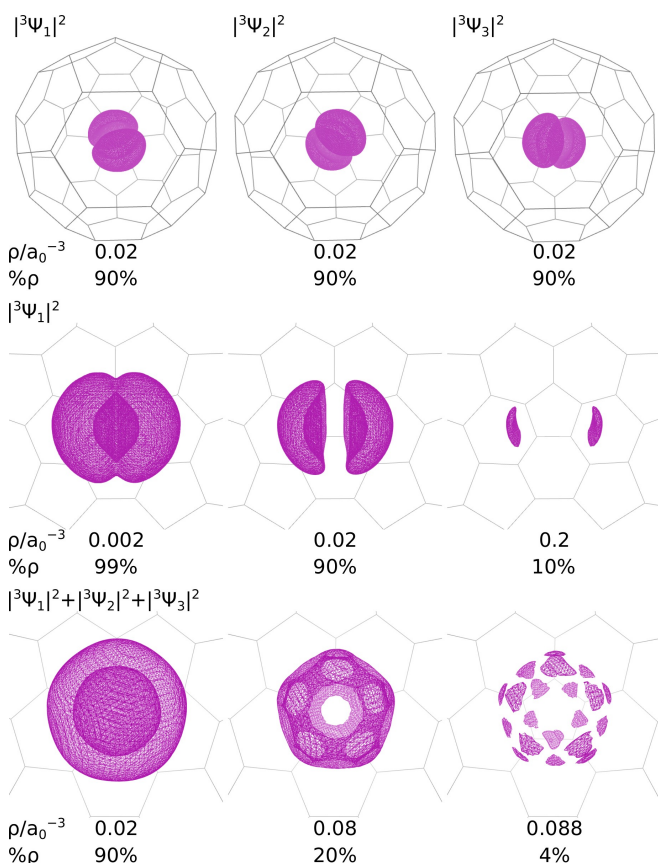


Figure 5. Density contours for the three lowest energy NC-NOCI $o\text{-He}_2@C_{60}$ states (top). Selected contour values for one state density (middle). Selected contour values for the average of the three densities (bottom). NC-NOCI calculations obtained from 194 possible He positions with the [1s1p1d] basis set.

with the isotropic HO plus RR \hat{H}_0 hamiltonian and the nearly spherical densities observed in the NC-NOCI. However, the NC-NOCI method provides a more comprehensive description of the density distributions, as it correctly responds to the icosahedral symmetry of the external potential.

Rotational and translational excited states

Figure 6 presents an energy diagram with the NC-NOCI and the PT-HORR predictions for the first $\text{He}_2@C_{60}$ excited states. The first NC-NOCI $p\text{-He}_2$ excited states are five-fold degenerate, with a relative energy only 0.8 cm^{-1} lower than the PT states with $l=0, j=2$. In contrast, the first excited state of $o\text{-He}_2$ does not exhibit the expected seven-fold degeneracy of a $\lambda=3$ of a free RR state. Both the NC-NOCI and the PT approaches predict the splitting of the $l=0, j=3$ manifold into four and three degenerate states. The energy differences in the NC-NOCI and PT predictions are 1.0 and 1.3 cm^{-1} , respectively.

The anticipated lifting of the degeneracy of spherical harmonics by an external field aligns with its corresponding symmetry.^[83,84] Inspecting the character table of the I_h point group,^[84] we observe that spherical harmonics with $\lambda=1$ and $\lambda=2$ conform to the irreducible representations T_{1u} and H_g , respectively. On the contrary, for $\lambda=3$, three states have G_u and four have T_{2u} symmetries. Consequently, the external I_h potential does not lift the degeneracy of the $\lambda=1$ and $\lambda=2$ rotational states, whereas it lifts the degeneracy of the $\lambda=3$ manifold into the G_u and T_{2u} states. These “crystal field”

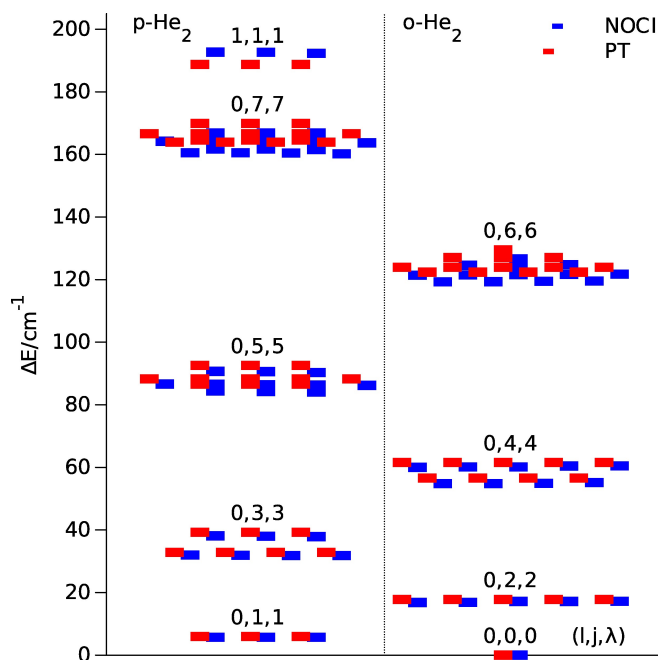


Figure 6. Relative energy diagram for the 85 first NC-NOCI and PT-HORR states of $\text{He}_2@C_{60}$. Differences with respect to the NC-NOCI (7.253 mE_h) and PT-HORR (7.151 mE_h) $p\text{-He}_2@C_{60}$ ground-state energies. The manifolds are labeled according to the PT-HORR quantum numbers l, j, λ , with $n=l$. NC-NOCI calculations obtained from 194 possible He positions with the [1s1p1d] basis set.

splittings, known as m_λ splittings, have also been observed in $\text{H}_2@\text{C}_{60}$.^[55]

Further inspection of Figure 6 reveals that the NC-NOCI and PT approaches predict similar I_h symmetry-induced m_λ splittings for the $l=0, j=4$ to $l=0, j=7$ manifolds. For these states, the predicted NC-NOCI energies are marginally lower, approximately 2 to 3%, in contrast to the PT-HORR outcomes. These results expose the capability of the proposed NC-NOCI method to effectively capture the response of excited nuclear wavefunctions to the symmetry of the external potential.

The three highest NC-NOCI states in Figure 6 correspond to the PT-HORR excited translational manifold, characterized by $l=1, j=1, j=1$. These excited translational states illustrate the coupling between the translational and rotational angular momenta. The nine-state manifold with $l=1$ and $j=1$ splits into three distinct manifolds, according to the corresponding total angular momentum λ . As detailed in Table S6 within the SI, the PT method yields energy values of 328, 189 and 245 cm⁻¹ for $\lambda=0, 1$, and 2, respectively. The observed energy order within this manifold echoes the behavior observed in $\text{H}_2@\text{C}_{60}$ where a similar splitting caused by the $I+j$ angular momentum coupling is referred to as λ splitting.^[55]

In Figure S7 in the SI we present a comparison of the first 90 *p*-He₂ and *o*-He₂ states computed with our NC-NOCI method alongside the PT-HORR results. For states with a relative energy greater than 200 cm⁻¹, the agreement between NOCI and PT is not as consistent as previously discussed. There are some differences in the degeneracy patterns and the state ordering, with up to 9% discrepancy in the energies. Still, there are a high number of *ortho*- and *para*- states coinciding with comparable energies. This semiquantitative agreement provides evidence that the NC-NOCI results include effects from the $I+j$ angular momentum coupling in translational excited states.

Finally, we highlight some differences between the low-energy states observed in He₂@C₆₀ and H₂@C₆₀. Previous studies have demonstrated that the former system behaves as a free rotor confined in a nearly spherical harmonic potential. For this comparison, we consider our PT results and the H₂ PT states presented in Ref. [55]. Both systems display similar translational frequencies, around 180 cm⁻¹ in H₂@C₆₀ and 230 cm⁻¹ in He₂@C₆₀. However, they show contrasting rotational constants: 55 cm⁻¹ for H₂ and only 2.9 cm⁻¹ for the He₂ pseudo-molecule, attributed to the longer He-He equilibrium distance (3.658 a₀), in contrast to the H-H bond length (1.476 a₀). Consequently, the first excited states of *p*-H₂@C₆₀ and *o*-H₂@C₆₀ are $n=l=1$ translational excited states, with $j=0, \lambda=1$, and $j=1, \lambda=1$ respectively, and display λ splitting. In contrast, as depicted in Figure 6, the rotational excitations in He₂@C₆₀ demand significantly less energy compared to their translational counterparts. This difference leads to the observation that in He₂@C₆₀ the m_λ splitting in the translational ground state occurs at lower energies than λ splitting in translational excited states.

Another significant difference between He₂@C₆₀ and H₂@C₆₀ is the magnitude of the λ and m_λ splittings. In the lowest energy manifold with λ splitting ($n=l=1, j=1$), the $\lambda=1$ and $\lambda=2$ states are separated by 6.5 cm⁻¹ in H₂@C₆₀ and by 61 cm⁻¹ in He₂@C₆₀. Similarly, the lowest energy manifold with m_λ

splitting in H₂@C₆₀ ($n=l=2, j=1, j=3$) has a separation of 0.5 cm⁻¹, while in He₂@C₆₀ ($n=l=0, j=3, \lambda=3$) the separation is 6.1 cm⁻¹. The increased magnitude of the λ and m_λ splittings is a consequence of the shorter average distance between the He atoms and the C₆₀ wall, which results in a stronger repulsive interaction and intensifies the impact of the potential anisotropy in the He₂@C₆₀ energies.

An imminent step in our research involves computing the NC-NOCI energy states of H₂@C₆₀ and H₂O@C₆₀, followed by a comprehensive comparison with existing theoretical and experimental data.^[55,65,67,85,86] However, these upcoming studies will face additional challenges in the description of hydrogen nuclei with a pairwise pseudo-particle approach. Specifically, the description of the H-C₆₀ interaction, detailed in Ref. [58], requires an additional Lennard-Jones center positioned in the middle of the H-H bond, and poses compatibility issues with the current NC-NOCI orbital framework. In addition, at extended H-H separations, each H exhibits radical-like behavior, characterized by an entirely distinct potential. The case of H₂O@C₆₀ introduces an additional layer of complexity because its center of mass does not coincide with the heavier oxygen nucleus.

Conclusions

We have conducted a study on the energies and structure of two ³He atoms trapped in C₆₀, utilizing a Hamiltonian that draws parallels between endohedral systems and many-electron atoms. In this Hamiltonian, the interactions of the trapped particles are represented by effective NC potentials. When employing the HF method to obtain He wavefunctions, our results demonstrate that spin and spatial symmetries are broken to lower the energy. To ensure wavefunctions with the correct symmetries, we employed a NC-NOCI method, which mixes the broken-symmetry HF wavefunctions.

For the *p*-He₂@C₆₀ system, our NC-NOCI predicts a ground state that displays an A_g singlet configuration. For *o*-He₂@C₆₀, the ground state is triply degenerate with T_{1u} symmetry, and is 5.69 cm⁻¹ higher in energy compared to *p*-He₂@C₆₀. These observations are in close agreement with the expected symmetries and energies obtained with a PT approach, based on a HO plus RR model, which predicts a 5.93 cm⁻¹ *o*-*p* energy difference. Furthermore, the NC-NOCI nuclear densities obtained for *p*-He₂ and *o*-He₂ display the icosahedral symmetry of the C₆₀ embedding potential. In addition, the energies of the first NC-NOCI and PT-HORR excited states display the expected splitting pattern derived from a symmetry analysis of the spherical harmonics interacting with an external icosahedral field.

To the best of our knowledge, this is the first theoretical study that highlights the relevance of the fermionic nature of ³He nuclei in describing confined He atoms within fullerenes. Given that He₂@C₆₀ has been detected^[26] and synthesized,^[27] it may be feasible to experimentally determine the *o*-*p* splitting in ³He₂@C₆₀.

In future research, we plan to investigate endohedral systems with three or more He nuclei to explore the possible

formation of nuclear shells, similar to what is observed in the electronic structure of atoms. We will also perform calculations on other fullerenes holding two He atoms,^[87] to analyze the impact of different encapsulating symmetries on the *o-p* splitting.

It is important to note that while the proposed method may not be as accurate as other approaches used to describe the quantum nature of endohedral atoms and molecules,^[88] such as FCI^[54] and multiconfigurational time-dependent Hartree^[85] approaches, it offers generality.

The NC Hamiltonian employed, and the NC-NOCI implementation in the openLOWDIN code is not limited to the system studied in this manuscript. Instead, it can be applied to describe any embedded system with any number of particles, where the interactions can be physically represented through pairwise potentials. Thus, the proposed approach can be used to investigate nuclear quantum effects of a variety of confined species affected by effective isotropic or anisotropic potentials. Of particular interest to us is the application of this methodology to analyze the energy splitting of *p*-H₂O and *o*-H₂O in different chemical environments.

Supporting Information

Additional equations, figures and tables are collected in the Supporting Information, providing: the GTFs fitted parameters to the potentials; the C₆₀ coordinates; details of the PT angular wavefunctions and energy expectation integrals; a list of the NC-NOCI and PT-HORR computed energies. Additional references have been cited within the Supporting Information.^[89–91]

Acknowledgements

FM and LGMP acknowledge financial support from the European Research Council (ERC) Advanced Grant under Project No. 101021166 – GAS-WAT. AR acknowledges the financial support of the Office of Research of the National University of Colombia (QUIPU codes: 400000035813, 201010040226) WQ acknowledges the financial support of the ANID/Doctorado Nacional/21222021 Ph.D. fellowship. The computations were enabled by resources provided by the National Academic Infrastructure for Supercomputing in Sweden (NAIIS) at the National Supercomputer Center at Linköping (NSC) partially funded by the Swedish Research Council through grant agreement no. 2022-06725.

Conflict of Interests

The authors declare no conflict of interest.

Data Availability Statement

The data that support the findings of this study are available in the supplementary material of this article.

Keywords: ab initio calculations • fullerenes • isotope effects • nuclear quantum effects • quantum chemistry

- [1] T. Miyazaki, *Atom tunneling phenomena in physics, chemistry and biology*, volume 36, Springer Science & Business Media **2004**.
- [2] M. Wolfberg, W. Van Hook, P. Paneth, L. Rebelo, *Isotope Effects: in the Chemical, Geological, and Bio Sciences*, Springer Netherlands **2009**.
- [3] J. Kästner, S. Kozuch, Tunnelling in Molecules: Nuclear Quantum Effects from Bio to Physical Chemistry, ISSN, Royal Society of Chemistry **2020**.
- [4] T. Ishimoto, M. Tachikawa, U. Nagashima, *Int. J. Quantum Chem.* **2009**, *109*, 2677.
- [5] N. F. Aguirre, P. Villarreal, G. Delgado-Barrio, E. Posada, A. Reyes, M. Biczysko, A. O. Mitrushchenkov, M. P. de Lara-Castells, *J. Chem. Phys.* **2013**, *138*.
- [6] M. Ceriotti, W. Fang, P. G. Kusalik, R. H. McKenzie, A. Michaelides, M. A. Morales, T. E. Markland, *Chem. Rev.* **2016**, *116*, 7529.
- [7] T. E. Markland, M. Ceriotti, *Nat. Chem. Rev.* **2018**, *2*.
- [8] F. Pavošević, T. Culpitt, S. Hammes-Schiffer, *Chem. Rev.* **2020**, *120*, 4222.
- [9] G. Cassone, *J. Phys. Chem. Lett.* **2020**, *11*, 8983.
- [10] A. Kundu, Y. Song, G. Galli, *Proc. Natl. Acad. Sci. USA* **2022**, *119*, e2203083119.
- [11] N. J. Turro, *Proc. Natl. Acad. Sci. USA* **1983**, *80*, 609.
- [12] E. A. Chekhovich, M. N. Makhonin, A. I. Tartakovskii, A. Yacoby, H. Bluhm, K. C. Nowack, L. M. K. Vandersypen, *Nat. Mater.* **2013**, *12*, 494.
- [13] J. B. Lambert, E. P. Mazzola, C. D. Ridge, *Nuclear Magnetic Resonance Spectroscopy: An Introduction to Principles, Applications, and Experimental Methods*, Wiley **2019**.
- [14] A. Schweiger, G. Jeschke, *Principles of Pulse Electron Paramagnetic Resonance*, Oxford University Press **2001**.
- [15] C. Puzzarini, J. F. Stanton, J. Gauss, *Int. Rev. Phys. Chem.* **2010**, *29*, 273.
- [16] U. Ranieri, M. M. Koza, W. F. Kuhs, R. Gaal, S. Klotz, A. Falenty, D. Wallacher, J. Ollivier, P. Gillet, L. E. Bove, *J. Chem. Phys. C* **2019**, *123*, 1888.
- [17] J. Tennyson, P. F. Bernath, L. R. Brown, A. Campargue, A. G. Császár, L. Daumont, R. R. Gamache, J. T. Hodges, O. V. Naumenko, O. L. Polyansky, et al., *J. Quant. Spectrosc. Radiat. Transfer* **2013**, *117*, 29.
- [18] P. Villarreal, M. de Lara-Castells, R. Prosmitsi, G. Delgado-Barrio, D. López-Durán, F. A. Gianturco, J. Jellinek, *Phys. Scr.* **2007**, *76*, C96.
- [19] D. S. Miyoshi, R. M. Cotts, A. S. Greenberg, R. C. Richardson, *Phys. Rev. A* **1970**, *2*, 870.
- [20] A. S. Dickinson, F. X. Gadéa, T. Leininger, *J. Phys. B At. Mol. Opt. Phys.* **2004**, *37*, 587.
- [21] J. P. Toennies, A. F. Vilesov, *Angew. Chem. Int. Ed.* **2004**, *43*, 2622.
- [22] Y. Moriwaki, N. Morita, *Eur. Phys. J. D* **2005**, *33*, 32.
- [23] S. Grebenev, J. P. Toennies, A. F. Vilesov, *Science* **1998**, *279*, 2083.
- [24] J. Harms, M. Hartmann, B. Sartakov, J. P. Toennies, A. F. Vilesov, *J. Chem. Phys.* **1999**, *110*, 5124.
- [25] U. Even, I. Al-Hroub, J. Jortner, *J. Chem. Phys.* **2001**, *115*, 2069.
- [26] T. Sternfeld, R. E. Hoffman, M. Saunders, R. J. Cross, M. Syamala, M. Rabinovitz, *J. Am. Chem. Soc.* **2002**, *124*, 8786.
- [27] R.-F. Peng, S.-J. Chu, Y.-M. Huang, H.-J. Yu, T.-S. Wang, B. Jin, Y.-B. Fu, C.-R. Wang, *J. Mater. Chem.* **2009**, *19*, 3602.
- [28] Y. Morinaka, S. Sato, A. Wakamiya, H. Nikawa, N. Mizorogi, F. Tanabe, M. Murata, K. Komatsu, K. Furukawa, T. Kato, et al., *Nat. Commun.* **2013**, *4*, 1554.
- [29] G. R. Bacanu, T. Jafari, M. Aouane, J. Rantaharju, M. Walkey, G. Hoffman, A. Shugai, U. Nagel, M. Jiménez-Ruiz, A. J. Horsewill, et al., *J. Chem. Phys.* **2021**, *155*.
- [30] L. Pang, F. Brisse, *J. Phys. Chem.* **1993**, *97*, 8562.
- [31] M. Straka, J. Vaara, *J. Phys. Chem. A* **2006**, *110*, 12338.
- [32] A. Krapp, G. Frenking, *Chem. Eur. J.* **2007**, *13*, 8256.
- [33] E. Cerpa, A. Krapp, R. Flores-Moreno, K. J. Donald, G. Merino, *Chem. Eur. J.* **2009**, *15*, 1985.
- [34] A. A. Popov, S. Yang, L. Dunsch, *Chem. Rev.* **2013**, *113*, 5989.
- [35] J. Vicha, J. Vaara, M. Straka, *Phys. Chem. Chem. Phys.* **2023**, *25*, 10620.
- [36] S. Jalife, J. Arcudia, S. Pan, G. Merino, *Chem. Sci.* **2020**, *11*, 6642.
- [37] S. Osuna, M. Swart, M. Solá, *Chem. Eur. J.* **2009**, *15*, 13111.

- [38] M. Khatua, S. Pan, P. K. Chattaraj, *Chem. Phys. Lett.* **2014**, *610*, 351.
- [39] P. Å Malmqvist, *Int. J. Quantum Chem.* **1986**, *30*, 479.
- [40] A. J. W. Thom, M. Head-Gordon, *J. Chem. Phys.* **2009**, *131*.
- [41] E. J. Sundstrom, M. Head-Gordon, *J. Chem. Phys.* **2014**, *140*.
- [42] J. H. Skone, M. V. Pak, S. Hammes-Schiffer, *J. Chem. Phys.* **2005**, *123*.
- [43] P. Jungwirth, A. I. Krylov, *J. Chem. Phys.* **2001**, *115*, 10214.
- [44] F. A. Gianturco, F. Paesani, I. Bacarelli, G. Delgado-Barrio, T. González-Lezana, S. Miret-Artés, P. Villarreal, G. Bendazzoli, S. Evangelisti, *J. Chem. Phys.* **2001**, *114*, 5520.
- [45] A. Heidenreich, U. Even, J. Jortner, *J. Chem. Phys.* **2001**, *115*, 10175.
- [46] D. López-Durán, M. P. de Lara-Castells, G. Delgado-Barrio, P. Villarreal, C. Di Paola, F. A. Gianturco, J. Jellinek, *Phys. Rev. Lett.* **2004**, *93*, 53401.
- [47] M. de Lara-Castells, D. López-Durán, G. Delgado-Barrio, P. Villarreal, C. Di Paola, F. A. Gianturco, J. Jellinek, *Phys. Rev. A* **2005**, *71*, 033203.
- [48] M. P. de Lara-Castells, G. Delgado-Barrio, P. Villarreal, A. O. Mitrushchenkov, *J. Chem. Phys.* **2006**, *125*, 221101.
- [49] M. P. de Lara-Castells, R. Prosmitti, D. López-Durán, G. Delgado-Barrio, P. Villarreal, F. A. Gianturco, J. Jellinek, *Int. J. Quantum Chem.* **2007**, *107*, 2902.
- [50] M. de Lara-Castells, P. Villarreal, G. Delgado-Barrio, A. O. Mitrushchenkov, *J. Chem. Phys.* **2009**, *131*.
- [51] M. de Lara-Castells, A. O. Mitrushchenkov, G. Delgado-Barrio, P. Villarreal, *Few-Body Syst.* **2009**, *45*, 233.
- [52] A. Valdés, R. Prosmitti, P. Villarreal, G. Delgado-Barrio, *J. Phys. Chem. A* **2012**, *116*, 7169.
- [53] N. F. Aguirre, P. Villarreal, G. Delgado-Barrio, A. O. Mitrushchenkov, M. P. de Lara-Castells, *Phys. Chem. Chem. Phys.* **2013**, *15*, 10126.
- [54] M. P. de Lara-Castells, A. O. Mitrushchenkov, *Phys. Chem. Chem. Phys.* **2021**, *23*, 7908.
- [55] P. M. Felker, Z. Bačić, *J. Chem. Phys.* **2016**, *145*, 084310.
- [56] M. Xu, F. Sebastianelli, Z. Bačić, R. Lawler, N. J. Turro, *J. Chem. Phys.* **2008**, *128*, 011101.
- [57] M. Xu, F. Sebastianelli, Z. Bacic, R. Lawler, N. Turro, *J. Chem. Phys.* **2008**, *129*, 64313.
- [58] M. Xu, F. Sebastianelli, B. R. Gibbons, Z. Bacic, R. Lawler, N. J. Turro, *J. Chem. Phys.* **2009**, *130*, 224306.
- [59] S. Mamone, M. Ge, D. Hüvonen, U. Nagel, A. Danquigny, F. Cuda, M. C. Grossel, Y. Murata, K. Komatsu, M. H. Levitt, et al., *J. Chem. Phys.* **2009**, *130*, 81103.
- [60] A. J. Horsewill, S. Rols, M. R. Johnson, Y. Murata, M. Murata, K. Komatsu, M. Carravetta, S. Mamone, M. H. Levitt, J. Y.-C. Chen, J. A. Johnson, X. Lei, N. J. Turro, *Phys. Rev. B* **2010**, *82*, 081410.
- [61] S. Mamone, J. Y.-C. Chen, R. Bhattacharyya, M. H. Levitt, R. G. Lawler, A. J. Horsewill, T. Röööm, Z. Bačić, N. J. Turro, *Coord. Chem. Rev.* **2011**, *255*, 938.
- [62] M. Ge, U. Nagel, D. Hüvonen, T. Röööm, S. Mamone, M. H. Levitt, M. Carravetta, Y. Murata, K. Komatsu, X. Lei, N. J. Turro, *J. Chem. Phys.* **2011**, *135*, 114511.
- [63] M. Ge, U. Nagel, D. Hüvonen, T. Röööm, S. Mamone, M. H. Levitt, M. Carravetta, Y. Murata, K. Komatsu, J. Y.-C. Chen, N. J. Turro, *J. Chem. Phys.* **2011**, *134*, 054507.
- [64] M. Xu, S. Ye, A. Powers, R. Lawler, N. J. Turro, Z. Bačić, *J. Chem. Phys.* **2013**, *139*, 064309.
- [65] T. Röööm, L. Peedu, M. Ge, D. Hüvonen, U. Nagel, S. Ye, M. Xu, Z. Bačić, S. Mamone, M. H. Levitt, M. Carravetta, J.-C. Chen, X. Lei, N. J. Turro, Y. Murata, K. Komatsu, *Philos. Trans. R. Soc. London Ser. A* **2013**, *371*, 20110631.
- [66] A. J. Horsewill, K. S. Panesar, S. Rols, J. Ollivier, M. R. Johnson, M. Carravetta, S. Mamone, M. H. Levitt, Y. Murata, K. Komatsu, J. Y.-C. Chen, J. A. Johnson, X. Lei, N. J. Turro, *Phys. Rev. B* **2012**, *85*, 205440.
- [67] A. J. Horsewill, K. Goh, S. Rols, J. Ollivier, M. R. Johnson, M. H. Levitt, M. Carravetta, S. Mamone, Y. Murata, J. Y.-C. Chen, J. A. Johnson, X. Lei, N. J. Turro, *Philos. Trans. Royal Soc. A* **2013**, *371*, 20110627.
- [68] C. G. Joslin, C. G. Gray, J. D. Goddard, S. Goldman, J. Yang, J. D. Poll, *Chem. Phys. Lett.* **1993**, *213*, 377.
- [69] C. G. Joslin, J. Yang, C. G. Gray, S. Goldman, J. D. Poll, *Chem. Phys. Lett.* **1993**, *208*, 86.
- [70] M. Zhang, L. B. Harding, S. K. Gray, S. A. Rice, *J. Phys. Chem. A* **2008**, *112*, 5478.
- [71] A. W. Hauser, A. O. Mitrushchenkov, M. P. de Lara-Castells, *J. Phys. Chem. C* **2017**, *121*, 3807.
- [72] A. Szabo, N. Ostlund, *Modern Quantum Chemistry: Introduction to Advanced Electronic Structure Theory*, Dover Books on Chemistry, Dover Publications **2012**.
- [73] P.-O. Löwdin, *Phys. Rev.* **1955**, *97*, 1474.
- [74] K. Patkowski, G. Murdachaeuw, C. M. Fou, K. Szalewicz, *Mol. Phys.* **2005**, *103*, 2031.
- [75] J. Charry, E. Posada, F. Moncada, J. Romero, A. Reyes, openLOWDIN version 1.0.0 10.5281/zenodo.8125056 **2023**.
- [76] E. F. Valeev, Libint: A library for the evaluation of molecular integrals of many-body operators over Gaussian functions, <http://libint.valeev.net/> **2022**, version 2.8.0.
- [77] V. I. Lebedev, *Comput. Math. Math. Phys.* **1976**, *16*, 10.
- [78] R. Flores-Moreno, E. Posada, F. Moncada, J. Romero, J. Charry, M. Díaz-Tinoco, S. A. González, N. F. Aguirre, A. Reyes, *Int. J. Quantum Chem.* **2014**, *114*, 50.
- [79] A. Reyes, F. Moncada, J. Charry, *Int. J. Quantum Chem.* **2019**, *119*, e25705.
- [80] F. Neese, F. Wennmohs, U. Becker, C. Ripplinger, *J. Chem. Phys.* **2020**, *152*.
- [81] W. Humphrey, A. Dalke, K. Schulten, *J. Molec. Graphics* **1996**, *14*, 33.
- [82] A. Reyes, M. V. Pak, S. Hammes-Schiffer, *J. Chem. Phys.* **2005**, *123*, 64104.
- [83] H. Bethe, *Ann. Phys.* **1929**, *395*, 133.
- [84] U. Walter, *Phys. Rev. B* **1987**, *36*, 2504.
- [85] O. Carrillo-Bohórquez, Á. Valdés, R. Prosmitti, *J. Chem. Theory Comput.* **2021**, *17*, 5839.
- [86] A. Shugai, U. Nagel, Y. Murata, Y. Li, S. Mamone, A. Krachmalnicoff, S. Alom, R. J. Whithby, M. H. Levitt, T. Röööm, *J. Chem. Phys.* **2021**, *154*, 124311.
- [87] S. Gómez, A. Restrepo, *Phys. Chem. Chem. Phys.* **2019**, *21*, 15815.
- [88] P. M. Felker, Z. Bačić, *J. Chem. Phys.* **2020**, *152*.
- [89] A. C. Genz, A. A. Malik, *SIAM J. Numer. Anal.* **1983**, *20*, 580.
- [90] Wolfram Research, Inc., *Mathematica*, version 13.3, champaign, IL, **2023**.
- [91] H. T. Johansson, C. Forssén, *SIAM J. Sci. Comput.* **2016**, *38*, A376.

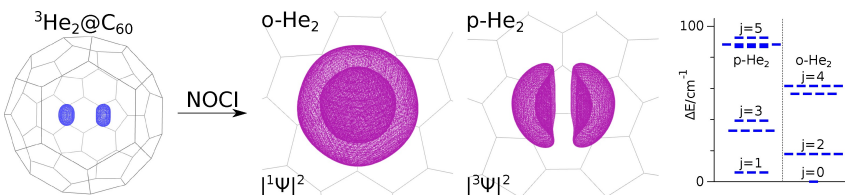
Manuscript received: July 13, 2023

Revised manuscript received: November 29, 2023

Accepted manuscript online: December 6, 2023

Version of record online: ■■■, ■■■

RESEARCH ARTICLE



We propose a non-orthogonal configuration interaction (NOCI) approach to investigate nuclear quantum effects of confined nuclei. With this approach, we obtain nuclear wavefunctions with correct spin and spatial

symmetries. We analyze the quantum states of two ^3He atoms encapsulated in C_{60} . The nuclear densities and energies correspond to a He_2 pseudo-molecule with nearly free rotation inside the C_{60} icosahedral potential.

F. Moncada, W. Quintero, E. Posada,
L. G. M. Pettersson, A. Reyes*

1 – 13

A nuclear configuration interaction approach to study nuclear spin effects: an application to *ortho*- and *para*- $^3\text{He}_2@\text{C}_{60}$



SPACE RESERVED FOR IMAGE AND LINK

Share your work on social media! *ChemPhysChem* has added Twitter as a means to promote your article. Twitter is an online microblogging service that enables its users to send and read short messages and media, known as tweets. Please check the pre-written tweet in the galley proofs for accuracy. If you, your team, or institution have a Twitter account, please include its handle @username. Please use hashtags only for the most important keywords, such as #catalysis, #nanoparticles, or #proteindesign. The ToC picture and a link to your article will be added automatically, so the **tweet text must not exceed 250 characters**. This tweet will be posted on the journal's Twitter account (follow us @ChemPhysChem) upon publication of your article in its final form. We recommend you to re-tweet it to alert more researchers about your publication, or to point it out to your institution's social media team.

ORCID (Open Researcher and Contributor ID)

Please check that the ORCID identifiers listed below are correct. We encourage all authors to provide an ORCID identifier for each coauthor. ORCID is a registry that provides researchers with a unique digital identifier. Some funding agencies recommend or even require the inclusion of ORCID IDs in all published articles, and authors should consult their funding agency guidelines for details. Registration is easy and free; for further information, see <http://orcid.org/>.

Félix Moncada <http://orcid.org/0000-0001-9701-2099>

William Quintero <http://orcid.org/0009-0007-1082-4096>

Edwin Posada <http://orcid.org/0000-0002-2565-0267>

Lars G. M. Pettersson <http://orcid.org/0000-0003-1133-9934>

Andrés Reyes <http://orcid.org/0000-0001-7571-2078>